Biochimica et Biophysica Acta 1804 (2010) 68–75

Contents lists available at ScienceDirect

Biochimica et Biophysica Acta

journal homepage: www.elsevier.com/locate/bbapap

Protein diffusion in crowded electrolyte solutions

Felix Roosen-Runge [a], Marcus Hennig [a,b], Tilo Seydel [b,*], Fajun Zhang [a], Maximilian W.A. Skoda [c], Stefan Zorn [a], Robert M.J. Jacobs [d], Marco Maccarini [b], Peter Fouquet [b], Frank Schreiber [a]

[a] Institut für Angewandte Physik, Universität Tübingen, D-72076 Tübingen, Germany
[b] Institut Laue-Langevin, B.P.156, F-38042 Grenoble, France
[c] ISIS, Rutherford Appleton Laboratory, Chilton, Didcot, UK
[d] Chemistry Research Laboratory, University of Oxford, Oxford, UK

ARTICLE INFO

Article history:
Received 16 March 2009
Received in revised form 2 June 2009
Accepted 3 July 2009
Available online 17 July 2009

Keywords:
Quasi-elastic neutron scattering
Cold neutron backscattering spectroscopy
Neutron spin echo spectroscopy
Globular proteins in aqueous solution
Salt ions

ABSTRACT

We report on a combined cold neutron backscattering and spin-echo study of the short-range and long-range nanosecond diffusion of the model globular protein bovine serum albumin (BSA) in aqueous solution as a function of protein concentration and NaCl salt concentration. Complementary small angle X-ray scattering data are used to obtain information on the correlations of the proteins in solution. Particular emphasis is put on the effect of crowding, i.e. conditions under which the proteins cannot be considered as objects independent of each other. We thus address the question at which concentration this crowding starts to influence the static and in particular also the dynamical behaviour. We also briefly discuss qualitatively which charge effects, i.e. effects due to the interplay of charged molecules in an electrolyte solution, may be anticipated. Both the issue of crowding as well as that of charge effects are particularly relevant for proteins and their function under physiological conditions, where the protein volume fraction can be up to approximately 40% and salt ions are ubiquitous. The interpretation of the data is put in the context of existing studies on related systems and of existing theoretical models.

1. Introduction

Proteins constitute the basis of the function of living cells. In addition to their structure, the dynamics of proteins is closely related to their biological function.

Some proteins occur in cell membranes, while others—the so-called globular ones—occur freely in water inside and outside the cells [1]. It is the latter category that the present article is concerned with. These globular proteins cannot be understood without their aqueous environment, and the ensemble of proteins and water may be denoted as a solution, suspension, or gel, depending on the physical—in particular viscoelastic—properties of the ensemble [2,3,4].

In a simplified picture, living cells operate through the motion of proteins embedded in a high-concentration ("crowded") aqueous solution of various macromolecules and salts [5]. Considerable debate therefore addresses the connection of protein function and protein motion in an aqueous environment as a function of environmental parameters such as charges and temperature. It can be assumed that protein function cannot be understood without taking into account protein motion in an aqueous environment and the interaction of proteins, ions, and water [6].

Neutron spectroscopy has since long been proven to be a useful tool to investigate protein dynamics [7]. While most other spectroscopic techniques, such as dynamic light scattering, are restricted to $Q \approx 0$, neutrons probe motion as a function of length scale from interatomic to mesoscopic distances in the sample, on time scales from sub-picoseconds to approximately 200 ns.

Most of the early neutron spectroscopy work concerning protein dynamics has been performed on powders or hydrated powder samples (for a review, see e.g. [8]). Interestingly, the biologically highly relevant case of protein solutions has rarely been studied, *inter alia* due to the difficulty of discriminating the contribution from the centre-of-mass diffusion of both protein and solvent molecules and also the problem of obtaining the required protein scattering volume while keeping the solvent scattering contribution low. Various studies indicate that protein dynamics in solution strongly depends on the external environment parameters, such as temperature, solution composition, concentration, ionic strength, and pH [9–15].

In addition to the issues related to solutions in general, the issue of crowding has to be observed. It is clear that with increasing protein concentration the protein–protein interaction becomes more relevant both for static and dynamic behaviours. However it is not at all obvious and also not well studied experimentally at which concentration the behaviour changes qualitatively. In other words: how concentrated does a protein solution have to be for crowding to impact the protein diffusion behaviour? Furthermore, crowding is

* Corresponding author.
E-mail address: seydel@ill.eu (T. Seydel).

1570-9639/$ – see front matter © 2009 Elsevier B.V. All rights reserved.
doi:10.1016/j.bbapap.2009.07.003

expected to be influenced by salt effects, since proteins in solution are generally charged, and the screening of these charges by salt ions has a profound impact on the effective interactions [16,17].

In the present article we report on our experiments on protein dynamics in crowded electrolyte solutions using high resolution quasi-elastic neutron scattering techniques, namely backscattering and spin-echo techniques. We discuss the results in the context of crowding and charge effects, i.e. effects due to the interplay of charged molecules in an electrolyte solution, on different length scales—i.e. on protein nearest neighbour distances and on intramolecular length scales—in the context of structural information obtained by applying small angle X-ray scattering (SAXS) techniques.

This article is organised as follows. After a short review of some theoretical concepts of diffusion in Section 2, the experimental details and data analysis procedures are explained in Section 3. In Section 4, first the (static) SAXS data are presented, followed by backscattering and neutron spin-echo (NSE) data. We attempt a comprehensive discussion in Section 5. A summary and conclusions are presented in Section 6.

2. Theory

For a general introduction into quasi-elastic neutron scattering we refer the reader to the textbooks by M. Bée and G.L. Squires [18,19]. Backscattering spectroscopy probes the incoherent scattering function S_{inc} and thus the ensemble-averaged motion of one single molecule, i.e., self-diffusion. In an idealised view, diffusion is referred to as Brownian motion of one particle experiencing no interactions except from stochastic forces due to solvent fluctuations which fulfill the fluctuation–dissipation theorem. This so-called free diffusion is described by the Langevin equation and yields a mean square displacement (MSD) linear in time:

$$W(t) = \langle |\boldsymbol{r}_1(0) - \boldsymbol{r}_1(t)|^2 \rangle = 6D_0 t, \tag{1}$$

hereby defining the diffusion coefficient D_0.

Since our experiments probe interacting particles (especially in crowded solutions), truly free diffusion is not seen. Nevertheless, in many experiments which probe only a certain time scale we obtain an MSD linear in time

$$W(t) = 6D_{\mathrm{app}} t, \tag{2}$$

where the apparent diffusion coefficient D_{app} is defined analogously to D_0.

2.1. Smoluchowski equation

The apparent diffusion can be treated according to a Langevin equation with additional interaction forces which operate rapidly when compared to the experimental time window. The aqueous medium causes a damping of motion, thus there exists a time scale on which the moments relax to zero. For BSA this so-called diffusive time scale equals

$$\tau_D \gg M\gamma \approx 2\ \mathrm{ps} \tag{3}$$

where $M = 66.43$ kDa is the mass of the BSA molecule and the friction parameter γ can be estimated from the dilute diffusion coefficient $D_0 = 6.62 \cdot 10^{-11}\ \mathrm{m^2 s^{-1}}$ [14] using the Einstein relation $D_0 = k_B T / \gamma$ at a given temperature ($T = 296$K).

A generalised description of motion on the diffusive time scale can be derived using the Smoluchowski equation, which describes the relaxation of interacting particles in a solvent experiencing a potential towards their equilibrium distribution. Bundling all position vectors $\boldsymbol{r}_l$ of the centres of mass of the molecules into one single configuration vector $\boldsymbol{r}$, the Smoluchowski equation describes the time evolution of the N particle distribution function $P(\boldsymbol{r}, t)$ by

$$\partial_t P(\boldsymbol{r}, t) = \nabla \cdot \mathbf{D}(\boldsymbol{r}) \cdot [\beta[\nabla V(\boldsymbol{r})] P(\boldsymbol{r}, t) + \nabla P(\boldsymbol{r}, t)] \tag{4}$$

where the diffusion tensor $\mathbf{D}$ characterises hydrodynamic interactions [20] and V is the total potential energy of all molecules. Diffusion coefficients are calculated by averaging over the probability density function P obtained from the Smoluchowski equation. This approach is applicable for our purposes, since the nanosecond time scale probed by neutron scattering is comparable to the diffusive time scale τ_D.

Due to the high protein concentration, which we investigate here, the molecules feel the presence of the surrounding molecules mediated by both hydrodynamic interactions and direct interactions. While the former interactions act quasi-instantaneously on the diffusive time scale, the latter are established on a longer time scale which is referred to as interaction time and can be estimated as

$$\tau_I = \frac{a^2}{D_0} \approx 100\ \mathrm{ns} \tag{5}$$

where $a \approx 2.8$ nm is the radius of one BSA molecule [20].

2.2. Self-diffusion

The self-diffusion coefficient D_s, which in general depends on both time t and the scattering vector $\boldsymbol{Q}$, is a measure of mobility of a single tracer molecule under the influence of intermolecular interactions and is linked to the incoherent intermediate scattering function by

$$I_{\mathrm{inc}}(\boldsymbol{Q}, t) = \langle e^{i\boldsymbol{Q}(\boldsymbol{r}_1(0) - \boldsymbol{r}_1(t))} \rangle = \exp\left\{ -D_s(\boldsymbol{Q}, t) \cdot \boldsymbol{Q}^2 t \right\} \tag{6}$$

where the angular brackets denote the averaging over the joint distribution $P(\boldsymbol{r}, \boldsymbol{r}_0, t) = P(\boldsymbol{r}, t|\boldsymbol{r}_0)\ P(\boldsymbol{r}_0)$. The conditional distribution $P(\boldsymbol{r}, t|\boldsymbol{r}_0)$ is the solution of the Smoluchowski equation given that the molecules were initially in the configuration $\boldsymbol{r}_0$ and $P(\boldsymbol{r}_0)$ is the Boltzmann distribution for the potential function.

In the short-time limit $\tau \ll \tau_I$ the molecules diffuse a short distance on the order of their own size influenced only by the quasi-instantaneously acting hydrodynamic interactions. Direct interactions play a less important role, since the potential does not change on the corresponding length scale. Thus, short-time self-diffusion can be understood intuitively as relatively free diffusion on a length scale limited by the direct interactions, while the hydrodynamic interactions act via a change of the effective solvent viscosity. Expanding both sides of Eq. (6) in time and neglecting higher order terms, i.e. in the short-time limit, the MSD reads $W(t) = \langle |\boldsymbol{r}_1(t) - \boldsymbol{r}_1(0)|^2 \rangle = 6D_s^s t$. Here the short-time self-diffusion coefficient D_s^s turns out to be independent from time and $\boldsymbol{Q}$.

2.3. Collective diffusion

Unlike self-diffusion, collective diffusion relates to the motion of many Brownian particles simultaneously and describes in the small $\boldsymbol{Q}$ limit the relaxation of the macroscopic density according to Fick's law [21]. Therefore, it is measured in a coherent experiment like dynamic light scattering or neutron spin-echo spectroscopy. The time and $\boldsymbol{Q}$ dependent collective diffusion coefficient D_c can be expressed by means of the coherent intermediate scattering function as follows [20,22]

$$S(\boldsymbol{Q}) \exp\left\{ -D_c(\boldsymbol{Q}, t) \cdot \boldsymbol{Q}^2 t \right\} = \frac{1}{N} \sum_{i,j=1}^{N} \left\langle \exp\left\{ i\boldsymbol{Q}\left(\boldsymbol{r}_i(0) - \boldsymbol{r}_j(t) \right) \right\} \right\rangle. \tag{7}$$

The importance of direct interactions is reflected in the appearance of the static structure factor $S(\boldsymbol{Q})$.

For large wave vectors $\boldsymbol{Q}$ the collective diffusion coefficient converges to the self-diffusion coefficient, because all cross-terms (those with $i \neq j$) become equal to zero, due to the rapidly oscillating behaviour of exp $\{i\boldsymbol{Q}(\boldsymbol{r}_i - \boldsymbol{r}_j)\}$ [11,22,23].

3. Experiments

3.1. Samples and measurements

Serum albumin is the most abundant protein in the blood plasma with an important role as stabilizer of both pH value and osmotic pressure of the blood. Furthermore, serum albumin acts as essential transport protein for a large variety of ligands, including fatty acids and metals [24]. The native concentration of serum albumin is typically 50 mg/ml, which corresponds to a volume fraction of 3.6%. The high solubility and availability of bovine serum albumin (BSA) and its importance as a multifunctional carrier make BSA a good model protein to study both collective and tracer diffusion in crowded solutions.

BSA was purchased from Sigma with an indicated purity of 99%. The protein was dissolved in D_2O at the desired NaCl and protein concentrations. Measurements of the pH value confirmed a constant pH in all samples of pH 6.93 ± 0.07. After preparation the protein solutions were left for several hours in the cold room to achieve complete solvation and equilibrium. Right before the measurement the solutions were filled into a cylindric thin-walled aluminium container (outer diameter 22 mm, gap width 0.3 mm) and sealed against vacuum.

Neutron backscattering spectroscopy data were collected at IN16 [25,26] (BSA volume fractions $\phi = 12.9\%$ and 27% corresponding to concentrations of 200 mg/ml and 500 mg/ml, respectively) and IN10 [26] ($\phi = 27\%$) at the ILL, Grenoble, both using cold neutrons with a wavelength of 6.27 Å and unpolished Si(111)-monochromators with a resolution of 0.9 μeV FWHM. The $\boldsymbol{Q}$ range was 0.43–1.93 $Å^{-1}$/0.5–1.96 $Å^{-1}$ with a dynamic range of ± 15 μeV / ± 10 μeV (IN16/IN10).

Neutron spin-echo scans were performed at IN11 [26,27] (BSA volume fractions $\phi = 3.6\%$ and 12.9% corresponding to concentrations of 50 mg/ml and 200 mg/ml, respectively) at the ILL, Grenoble, using wavelengths of 8.5 and 10 Å for $\boldsymbol{Q}$ vectors ranging from 0.04 to 0.2 $Å^{-1}$. Data sets were recorded for 280K (both NSE and backscattering) and 325K (only backscattering), respectively. In the $\boldsymbol{Q}$ range of up to 0.2 $Å^{-1}$ we were able to exploit the strong coherent small angle scattering signal of the samples with NSE. At higher $\boldsymbol{Q}$ values this is not possible anymore, the signal gets very weak and incoherent scattering becomes comparable in strength to coherent scattering or even dominant. We note that for the different experiments on NSE and backscattering spectrometers different cryostats have been used. Although the temperature sensors were calibrated, a systematic error in the absolute sample temperature of a few Kelvin may occur due to the distance between the temperature sensor on the tip of the stick holding the sample and the sample itself. In addition, different thermal conductivities may contribute to a systematic error.

The SAXS measurements were performed at Daresbury, UK, employing procedures similar to those of Ref. [16].

3.2. Data analysis

3.2.1. Backscattering

After normalisation of the backscattering data to the monitor spectrum, the spectra of pure D_2O were subtracted from the protein solution spectra. The bulk D_2O and the salt ions dissolved therein only contribute a constant signal, since their mobility is on picosecond time scales and therefore beyond the accessible dynamic window of a backscattering spectrometer. Therefore, we have neglected excluded-volume effects in the solvent subtraction. The instrumental resolution σ and the detector efficiency were determined detector-wise from the spectrum of vanadium measured in the sample geometry at $T = 280$K by a fit of a Gaussian and integration of the elastic line, respectively. This resolution was used as fixed parameter in the fits to the scattering function $S_{\mathrm{exp}}(\boldsymbol{Q},\omega)$ (Fig. 1). We used an approach with two Lorentzian line shapes (as used also in Refs.[28,29]).

The fit function can thus be written as

$$\begin{aligned} S_{\mathrm{fit}}(\boldsymbol{Q},\omega) &= \mathcal{R}(\omega,\sigma) \otimes [A(\boldsymbol{Q}) \cdot \mathcal{L}(\omega,\Gamma_1) + (1 - A(\boldsymbol{Q})) \cdot \mathcal{L}(\omega,\Gamma_2)] + B(\boldsymbol{Q}) \\ &= A(\boldsymbol{Q}) \cdot \mathcal{V}_{\Gamma_1,\sigma}(\omega) + (1 - A(\boldsymbol{Q})) \cdot \mathcal{V}_{\Gamma_2,\sigma}(\omega) + B(\boldsymbol{Q}), \end{aligned} \tag{8}$$

where $\mathcal{R}$ is the Gaussian resolution function with width σ, $\mathcal{L}$ is a Lorentzian function with half width at half maximum (HWHM) Γ, and $\mathcal{V}$, is a Voigt function [30–32]. $B(\boldsymbol{Q})$ is the background and $A(\boldsymbol{Q})$ is the quasi-elastic incoherent structure factor (QISF). The half width at half maximum (HWHM) of the second Lorentzian was fixed in our fits to $\Gamma_2 = 8$ μeV, assuming that this broad Lorentzian accounts for fast motions near the cut off due to the constant $\boldsymbol{Q}$-independent dynamic window of the spectrometer.

This model function can be interpreted as the combination of two dynamical processes, the centre-of-mass movement (diffusion in an unconfined medium) of the whole protein and other (faster) inter-

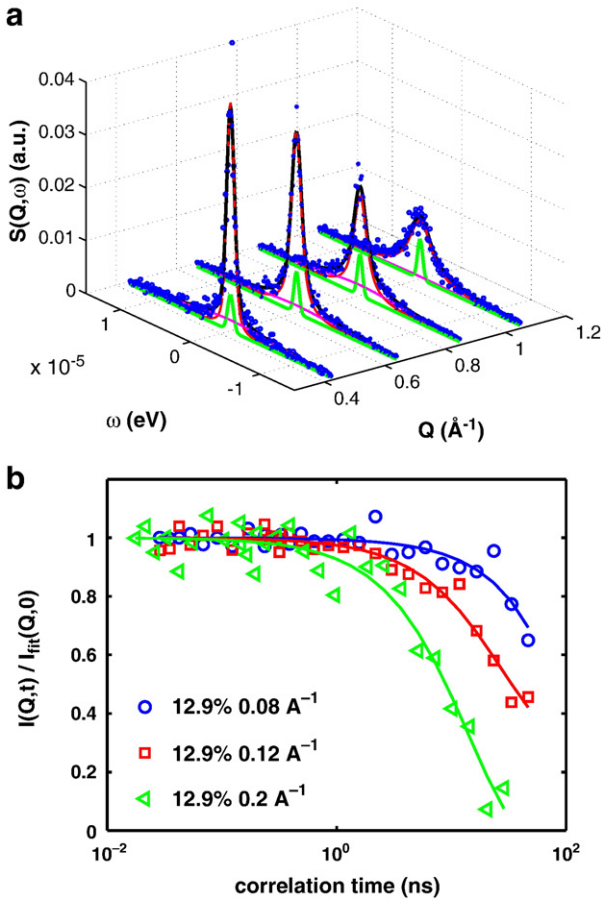

Fig. 1. (a) Backscattering spectra recorded at IN16, ILL, at different $\boldsymbol{Q}$ vectors for a BSA volume fraction of 12.9% without salt at $T = 280$K, after normalisation to the individual detector efficiencies. After the subtraction of the water background the data (blue symbols) can be fitted well by a model function (black line) consisting of two Lorentzians (red and magenta lines) convoluted with the Gaussian resolution function (green line). (b) Example correlation functions $I(\boldsymbol{Q}, t) / I_{\mathrm{fit}}(\boldsymbol{Q}, 0)$ derived from neutron spin-echo (NSE) scans for a BSA volume fraction of 12.9 % without salt. The fits are single exponentials.

domain and internal dynamics which are confined due to the protein topology:

$$S_{\mathrm{fit}} = S_{\mathrm{diff}} \otimes S_{\mathrm{internal}} = \mathcal{L}(\omega,\Gamma_{\mathrm{diff}}) \otimes [A(\mathbf{Q})\delta(\omega) + (1 - A(\mathbf{Q}))\mathcal{L}(\omega,\Gamma_{\mathrm{internal}})]. \quad (9)$$

In this interpretation the narrow Lorentzian corresponds to the global particle motion, whereas the broad Lorentzian consists of the convolution of both motions.

3.2.2. Error analysis

Different errors affect the experimental result. The counts I_k per energy channel k and detector exhibit a Poissonian distribution. Thus, normalisation to the monitor spectrum yields for the kth energy channel an error in intensity

$$\delta I_k = \Delta\left(\frac{N_k}{M_k}\right) = \frac{\sqrt{N_k}}{M_k} + \frac{N_k\sqrt{M_k}}{M_k^2}, \quad (10)$$

where N_k corresponds to the detector counts and M_k to the monitor counts, respectively.

The error of the experimental channel position due to a finite energy channel width ΔE can be approximated by the deviation of the mean energy of all counts in the kth channel:

$$\delta\omega_k = \sqrt{\frac{\langle\delta E^2\rangle}{N_k}} = \frac{\Delta E}{2\sqrt{3N_k}} \quad (11)$$

where

$$\langle\delta E^2\rangle = \int_{-0.5\Delta E}^{0.5\Delta E} dx \frac{x^2}{\Delta E} = \frac{\Delta E^2}{12} \quad (12)$$

corresponds to the deviation of one count (assuming a uniform distribution in each channel). Further error propagation is treated according to Gaussian error propagation.

3.2.3. Neutron spin-echo (NSE)

The neutron spin-echo data were processed by the standard IGOR routines (including fits and error analysis) used at IN11, ILL. NSE spectroscopy measures the real part of the normalised intermediate scattering function $\Re[I(\mathbf{Q},t) / I(\mathbf{Q},0)]$. In our case the imaginary part of $I(\mathbf{Q}, t)$ is negligible, so we measure, in fact, $I(\mathbf{Q}, t) / I(\mathbf{Q}, 0)$ [27]. The resolution correction in NSE is achieved by a simple division by the signal of an elastically scattering sample with the same sample geometry. We used graphite powder as the elastic sample.

The resolution corrected $I(\mathbf{Q}, t)$ data were fitted accurately by simple exponential decay curves $\exp(-t/\tau)$, where τ is the decay time of the relaxation. The Fourier transform of an exponential decay is a Lorentzian function as observed in the backscattering spectra with a corresponding quasi-elastic broadening (HWHM) given by $\Gamma = \hbar/\tau$ [18].

3.2.4. SAXS

With SAXS we measure the total scattering intensity $I(q)$, which for a monodisperse system can be expressed as

$$I(q) = N(\Delta\rho)^2 V^2 P(q) S(q), \quad (13)$$

where $S(q)$ is the structure factor, containing information about the intermolecular interaction, and $P(q)$, the so-called form factor, characterises the shape of the molecule. Furthermore, N is the number density of proteins and $\Delta\rho = \rho_P - \rho_s$ the electron density difference of the protein molecule and of the solvent, usually denoted scattering contrast. For an infinitely dilute solution the structure factor is unity. Hence, assuming a monodisperse system and a concentration independent form factor, we determined the form factor from a sufficiently dilute solution [16]. Finally, the total intensity data $I(q)$ were fitted using the structure factor

$$S(q) = 1 + 4\pi N \int_0^\infty [g(r) - 1] \frac{\sin(qr)}{qr} r^2 dr \quad (14)$$

via the Ornstein–Zernicke equation for different effective particle interactions, including the static pair-correlation function $g(r)$.

4. Results

4.1. Crowded aqueous solution of BSA—charge effect and SAXS

It is useful to first characterise the correlations and static (or so-called direct) interactions of crowded solutions by means of SAXS before examining their impact on dynamical properties. In previous SAXS measurements the static interactions of BSA in aqueous solutions has been systematically examined [16]. Here we focus on the effects which are related to crowding behaviour.

The low $\mathbf{Q}$ regime corresponds directly to the structure factor. Fig. 2 (a),(b) displays two typical scattering profiles for different protein and salt concentrations. For all samples without salt a pronounced

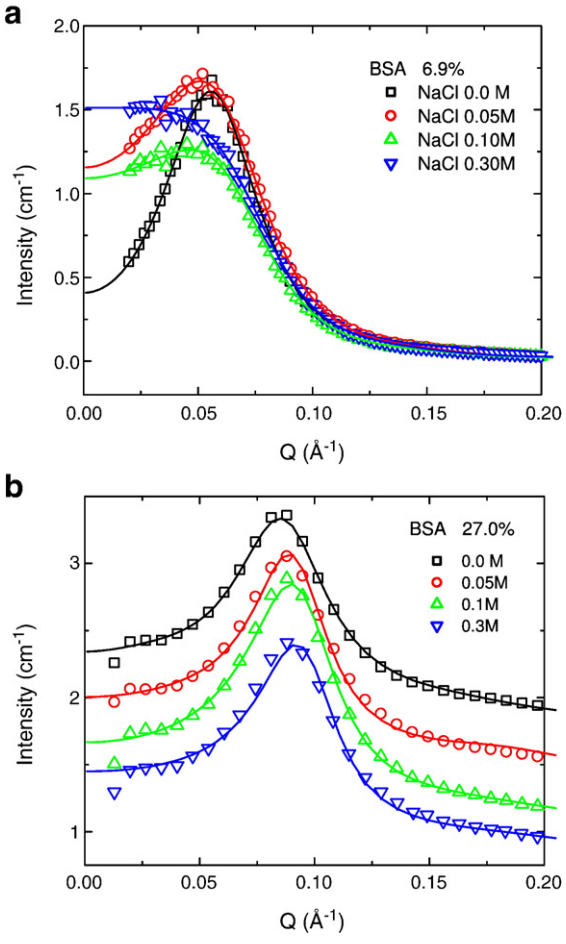

Fig. 2. Intensity data from SAXS measurements at BSA concentrations of 100 mg/ml (a) and 500 mg/ml (b) corresponding to volume fractions $\phi = 6.9\%$ (a) and 27% (b), respectively, for increasing NaCl concentrations. The data in (b) have been shifted along the intensity-axis for clarity. For low salt concentrations both show an intense correlation peak. While for increasing NaCl concentration this correlation peak disappears for BSA solutions at $\phi = 6.9\%$, the profile for $\phi = 27\%$ remains nearly unchanged upon increasing the salt concentration.

correlation peak is observed. The corresponding nearest neighbour distance $r_{c-c} = \frac{2\pi}{Q_{corr}}$ decreases upon increasing the concentration of BSA and is shown in Fig. 3. The line in the plot denotes the calculated nearest neighbour distance by simple geometrical consideration (see inset of Fig. 3) assuming a closest sphere packing of virtual spheres whose centres correspond to the equilibrium positions of the molecules:

$$r_{c-c} \approx \left(\frac{\phi/_{csp}}{\phi/}\right)^{\frac{1}{3}} 2\,a, \tag{15}$$

where $\phi_{csp} = \frac{\pi}{3\sqrt{(2)}} \approx 0.74$ corresponds to the volume fraction of the closest sphere packing, ϕ is the volume fraction of the molecules and $a \approx 2.8$ nm the effective radius of one molecule.

In Fig. 2(a), (b) the salt dependence of the scattering profile is shown for two crowded protein solutions (volume fractions 6.9% and 27 %, respectively). For the lower protein concentration the correlation peak disappears by addition of NaCl due to the salt screening effect. The interaction used for the fitting changes from a screened-Coulomb potential to an effective square-well potential. In contrast, for protein volume fractions above 13% the correlation peak is conserved upon addition of salt, and salt screening causes only a slight shift. The conservation of the correlation peak also for higher salt concentrations implies the absence of aggregation in this highly concentrated protein solution and indicates a behaviour corresponding to hard spheres in a random sphere packing (but not crystallinity).

4.2. Global motion of single BSA molecules in solution: backscattering

Fig. 1(a) shows a backscattering spectrum and the fit by two Lorentzian functions convoluted with a Gaussian resolution function. The derived widths Γ_1 of the narrow Lorentzian function for our fits are shown in Fig. 4(a) with a $\mathbf{Q}^2$ relationship for low $\mathbf{Q}$ according to simple diffusion. We note that for higher $\mathbf{Q}$ we see a sub-$\mathbf{Q}^2$ behaviour (sometimes taken as evidence for "jump diffusion"), which has also been observed in previous studies on proteins in crowded solutions by neutron backscattering [29], whereas there are several studies by time-of-flight spectroscopy in a comparable $\mathbf{Q}$ range which do not show this deviation [28,33]. This discrepancy suggests that the deviation is caused by the finite energy window of the spectrometer and therefore an inappropriate fitting model, but also real effects including crowding could be considered [29]. Since our backscattering

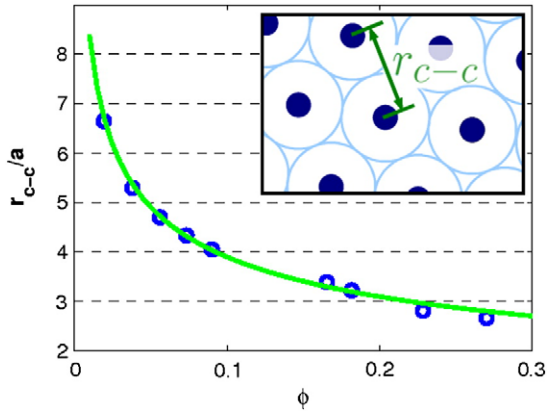

Fig. 3. Centre-to-centre distance $\mathbf{r}_{c-c}$ normalised to the effective radius $a = 2.8$ nm of BSA molecules in aqueous solution as a function of the BSA volume fraction ϕ obtained from SAXS data (circle symbols) and theoretical estimate according to Eq. (15) (line). By increasing the protein concentration the particles move closer together, as intuitively expected. The inset shows the geometrical consideration leading to Eq. (15): the equilibrium positions of the molecules (corresponding to the full spheres) are the centres of virtual spheres which establish a closest sphere packing.

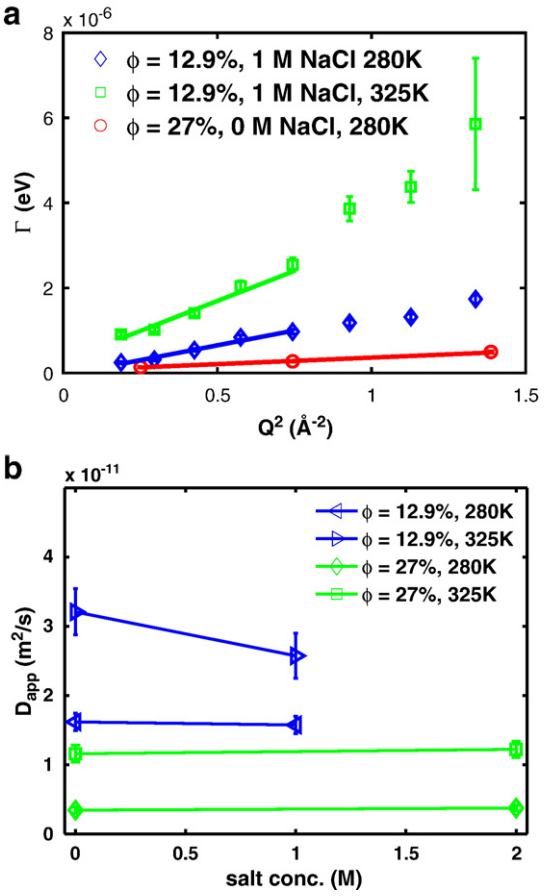

Fig. 4. Backscattering: (a) widths of the narrow Lorentzian versus $\mathbf{Q}^2$ for different protein concentrations which are derived as described in Section 2. The fit $\Gamma = D_{app}^{inc}\mathbf{Q}^2$ defines the apparent diffusion coefficient derived from backscattering spectroscopy, the fit range being restricted to the region where $\Gamma \propto \mathbf{Q}^2$ holds (see text). Data recorded on IN16 (square and diamond symbols) and IN10 (circle symbols). (b) Apparent diffusion constants versus NaCl concentration. While for different protein concentrations there are obvious differences in D_{app}^{inc}, the addition of salt appears to have little effect. (Corresponding data recorded on IN10 and IN16. The lines are guides to the eye.)

data do not provide further information on the nature of the deviation, we concentrate on the $\mathbf{Q}^2$ regime. We derive the apparent diffusion coefficient by a fit to the low $\mathbf{Q}$ regime: $\Gamma = D_{app}^{inc}Q^2$. For the samples with a BSA volume fraction $\phi = 12.9\%$ (measured at IN16) and $\phi = 27\%$ (IN10) we constrain the fit to $\mathbf{Q} < 0.85$ Å^{-1} and $\mathbf{Q} < 1.2$ Å^{-1}, respectively (Fig. 4(a)). The difference in the fit range accounts for the fact that the deviation from $\Gamma \propto \mathbf{Q}^2$ occurs for lower protein concentration already at lower $\mathbf{Q}$. We attribute this to the fact that at lower concentration (or higher temperature) the mobility becomes faster than detectable by the dynamic window of the spectrometer already at lower $\mathbf{Q}$.

In Fig. 4(b) the apparent diffusion coefficients are summarised. Two basic conclusions can be drawn: Firstly, in increasing the BSA concentration, the apparent diffusion is clearly slowed down. Secondly, the addition of NaCl has little or no effect for solutions with BSA volume fraction of 27%. For solutions with $\phi = 12.9\%$ there is a small decrease in diffusion upon addition of salt. We note that the choice of the width of the second, broad Lorentzian (see Section 2) has a systematic influence on the fit result for the narrow Lorentzian. An increase of the width of the broad Lorentzian results in a nearly constant shift of the apparent diffusion constants. However, this influence has little effect on the observed salt- and concentration-dependent trends. We motivate the choice of the value of 8 μeV for the HWHM of the broad Lorentzian by the dynamic range covered by the backscattering spectrometer (see Section 2).

4.3. Relaxation of fluctuations of BSA concentration in solution: NSE

In Fig. 1(b) three typical NSE spectra are depicted. The time window accessed by our experiment can be estimated from this figure (Fig. 1(b)), i.e. approximately 30 ps to 50 ns. All data sets are fitted well by a single exponential decay $I(\mathbf{Q}, t)/I(\mathbf{Q},0) \propto \exp(-t/\tau)$. The resulting decay times are summarised in Fig. 5(a). Assuming $H(\mathbf{Q})/S(\mathbf{Q}) = \text{const.}$ with the hydrodynamic function $H(Q)$ [22], the decay times τ can be related to a diffusion coefficient:

$$\frac{1}{\tau(\mathbf{Q})} = D_{\text{app}}^{\text{coh}}\mathbf{Q}^2. \tag{16}$$

$D_{\text{app}}^{\text{coh}}$ is the apparent diffusion coefficient, corresponding to the relaxation of fluctuations of BSA density [11,22,34]. The corresponding $\mathbf{Q}^2$ fits are shown as lines in Fig. 5(a). For the fit, the lowest value in $\mathbf{Q}$ has been ignored (see discussion below).

The apparent diffusion coefficients are shown in Fig. 5(b). Two trends can be observed: firstly, the apparent diffusion is slowed down with increasing protein concentration. Secondly, the addition of salt appears to slightly increase the diffusion in this regime.

5. Discussion

As the starting point for the discussion of the data we consider the SAXS data presented in Section 4.1. These provide information on equilibrium properties such as (averaged) particle–particle distances and effective interactions. Whereas for a protein volume fraction $\phi = 6.9\%$ the addition of salt changes the SAXS pattern, at a protein volume fraction $\phi = 27\%$ salt has little impact, indicating that at such a high concentration the solution is already rather crowded.

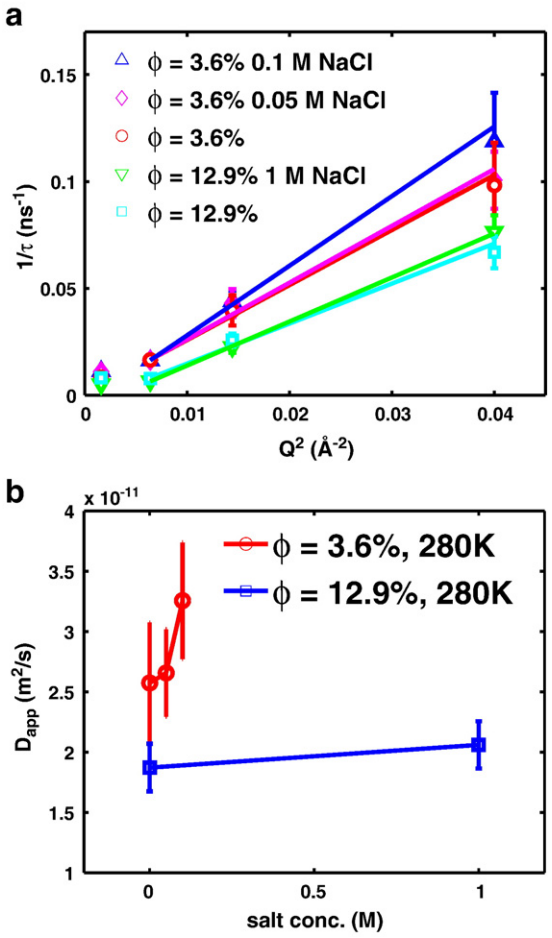

Fig. 5. NSE: (a) inverse decay times τ^{-1} for different experimental conditions. The linear fit $\tau^{-1} = D_{\text{app}}\mathbf{Q}^2$ yields an apparent diffusion coefficient derived from NSE. (b) Apparent diffusion coefficients versus NaCl concentration. Decreasing protein concentration and increasing salt concentration enhance the diffusion. (The lines in (b) are guides to the eye. The sample temperature was always $T = 280$K.)

Generally, one obvious effect of crowding is simply the excluded-volume effect, i.e., by increasing the protein concentration the particle–particle distance is decreased and thus the particle interactions become more important. We assume that for volume fractions above a certain value, spherical macromolecules whose interactions are dominated by strongly screened charges, i.e., close to the hard-sphere limit, organise in a pattern similar to random sphere packing. At this volume fraction the gap between two molecules drops below the diameter of one molecule, i.e. $\boldsymbol{r}_{c-c} < 4a$. We obtain for the corresponding volume fraction $\phi \approx \frac{\phi_{\text{csp}}}{8} = 9.25\%$ from Eq. (15). This qualitative change in the correlation of molecules is reflected in the appearance of a correlation peak in SAXS measurements at high concentrations of both protein ($\phi > 12\%$) and salt (above 0.5 M NaCl). For solutions without or with less salt, the correlation peak is observed already for very dilute solutions [16], indicating a long-range order of the time averaged position coordinates.

Concerning the change of dynamical behaviour of crowded solutions due to the excluded-volume effect, a strong concentration-dependence of the long-time self-diffusion is expected, again changing qualitatively at a volume fraction around 10% and including features like jump diffusion in the high concentration regime. In contrast, the short-time self-diffusion is expected to change continuously over the entire concentration range. In this time regime direct interactions are not relevant and the impact on the particle motions increases continuously starting from very low concentrations, as it is only mediated by long-ranged and quasi-instantaneously acting hydrodynamic interactions.

Apart from this behaviour, which on a qualitative level is not surprising, the screened-Coulomb interaction has additional effects on the issue of crowding. By increasing the salt concentration the screening length is decreased. Hence, the length scale on which direct interactions become important, the so-called interaction length scale λ_I, is decreased. This interaction length scale λ_I corresponds to a shortened interaction time scale $\tau_I \approx \frac{\lambda_I^2}{D_s^*}$. Thus, crowding in terms of an increased (screened-)Coulomb interaction causes a qualitative change in the dynamic behaviour.

Our neutron backscattering data show a $\mathbf{Q}^2$ relationship $\Gamma = D_{app}^{inc}\mathbf{Q}^2$ for $\mathbf{Q} \leq 1.2$ Å^{-1}. Upon increasing the protein concentration we observed a trend to slower diffusion, whereas salt seems to have little or no effect. The neutron spin-echo data show a $\mathbf{Q}^2$ relationship $\frac{1}{\tau} = D_{\text{app}}^{\text{coh}}\mathbf{Q}^2$. In contrast to backscattering data, we see an increase of diffusion upon addition of salt, whereas the dependence on protein concentration remains qualitatively the same, i.e., a decrease of apparent diffusion upon increasing protein concentration.

At this point, it is important to recall the similarities and the differences of backscattering and NSE, as well as the associated time and length scales. Generally, the neutron backscattering technique depends on incoherent scattering and thus studies self-diffusion. Since the interaction time $\tau \approx \frac{a^2}{D_0} \approx 100$ ns (Eq. (5)) is larger than our experimental time window, the derived apparent diffusion can be interpreted in terms of short-time self-diffusion. With this in mind, both observed trends are reasonable. While a variation of the protein concentration has a strong impact mediated by hydrodynamic interactions, the addition of salt yields only a slight variation. The latter can be rationalised as increase of the effective hydrodynamic radius due to the formation of the counter-ion layer [16,35].

Neutron spin-echo probes coherent scattering, thus in principle collective diffusion. The interaction time is close to the experimental

Table 1
Summary of apparent diffusion coefficients derived from our backscattering and neutron spin-echo experiments on BSA solutions (see text).

	ϕ	NaCl concentration	D (10^{-11} m^2/s)	
			280K	325K
NSE	3.6%	0 M	2.57 ± 0.50	
		0.05 M	2.66 ± 0.36	
		0.1 M	3.26 ± 0.48	
	12.9%	0 M	1.87 ± 0.20	
		1 M	2.06 ± 0.00	
Backscattering	12.9%	0 M	1.77 ± 0.13	4.44 ± 0.37
		1 M	1.73 ± 0.13	4.00 ± 0.35
	27%	0 M	0.422 ± 0.041	1.26 ± 0.12
		2 M	0.416 ± 0.040	1.33 ± 0.11

time window. Effects related to charge interactions are therefore expected. In our data this effect is reflected in the screening effect of salt. Importantly, in the high $\boldsymbol{Q}$ limit (i.e., $\boldsymbol{Q} \gg 2\pi r_c^{-1}$ $_c$), neutron spin-echo data can be interpreted effectively in terms of self-diffusion [11,22,23]. Since the nearest neighbour distances (see Fig. 3) are around 15 nm ($\phi = 3.6\%$) and 10 nm ($\phi = 12.9\%$), this approximation is fulfilled relatively well for the three higher $\boldsymbol{Q}$ values.

Both experiments agree quite well, as summarised in Table 1, evidencing a general slowing-down trend according to an excluded-volume interaction.

The dilute limit for the self-diffusion coefficient has been measured by dynamic light scattering in H_2O [14]. The derived $D_0 \approx 6.62 \cdot 10^{-11} \frac{m^2}{s}$ agrees well with an extrapolation of our observed trend towards the low concentration limit.

The different trends upon salt addition in our results are caused by different time regimes—while backscattering is in the short-time limit, neutron spin-echo probes time scales comparable to the interaction time.

6. Summary, conclusions, and outlook

We have presented a high resolution cold neutron scattering study of the dynamics of the model protein BSA in crowded aqueous solution as a function of the protein concentration and added salts. We have thus investigated molecular diffusion on nanosecond time scales in length scales ranging from protein nearest neighbour distances down to intramolecular length scales. These dynamical data have been combined with small angle X-ray scattering data on the same system.

From SAXS data we find a qualitative change from an uncorrelated to a strongly correlated solution due to increased excluded-volume effects. We conclude that below a volume fraction of approximately 10% crowding is induced by unscreened charges, whereas above that volume fraction crowding is dominated by the excluded-volume contribution. For weaker screening (i.e. less salt) this correlation is found already for lower protein concentrations.

For QENS data we find a continuously changing behaviour of the self-diffusion due to the excluded-volume effect. The addition of salt has little or no effect on the apparent diffusion coefficients, although charge screening is assumed to change both interaction time and coupling strength. In the protein concentration range covered by our experiments, i.e. from approximately 4% to 27% volume fraction, our data are in agreement with a continuous decrease of the apparent diffusion constants with the protein concentration. In contrast to the static data, our dynamic data show no distinct value where crowding due to the excluded-volume contribution sets in.

Understanding the dynamics of crowded solutions is not only a necessity to interpret QENS data, because usually these involve higher protein concentrations to achieve adequate statistics. Crowding itself, caused by a variety of hydrodynamic and direct interactions, is an important feature of cellular environments and has to be studied in further detail. We thus wish to prepare the ground for future experiments using multivalent salts giving rise to more complex phenomena such as the reentrant condensation [17] and the future extension to other protein systems.

Acknowledgements

Felix Roosen-Runge and Marcus Hennig gratefully acknowledge financial support from the ILL through studentships. The authors benefited from discussions with E. Reister (Stuttgart) and H. Schober (ILL, Grenoble).

References

[1] P. Lindgard, Reflections on the protein-folding problem, Journal of Physics: Condensed Matter 15 (18) (2003) S1779–S1786.
[2] J. Trevors, G. Pollack, Hypothesis: the origin of life in a hydrogel environment, Prog. Biophys. Mol. Biol. 89 (1) (2005) 1–8.
[3] K. Monkos, Viscosity of bovine serum albumin aqueous solutions as a function of temperature and concentration, Int. J. Biol. Macromol. 18 (1–2) (1996) 61–68.
[4] T. Hianik, S. Poniková, J. Bágelová, M. Antalík, Specific volume and compressibility of human serum albumin–polyanion complexes, Bioorg. Med. Chem. Lett. 16 (2) (2006) 274–279.
[5] R. Ellis, Macromolecular crowding: an important but neglected aspect of the intracellular environment, Curr. Opin. Struct. Biol. 11 (1) (2001) 114–119.
[6] P. Ball, Water as an active constituent in cell biology, Chem. Rev. 108 (1) (2008) 74–108.
[7] M. Bee, Localized and long-range diffusion in condensed matter: state of the art of QENS studies and future prospects, Chem. Phys. 292 (2–3) (2003) 121–141.
[8] F. Gabel, D. Bicout, U. Lehnert, M. Tehei, M. Weik, G. Zaccai, Protein dynamics studied by neutron scattering, Q. Rev. Biophys. 35 (04) (2003) 327–367.
[9] M. Placidi, S. Cannistraro, A dynamic light scattering study on mutual diffusion coefficient of BSA in concentrated aqueous solutions, Europhys. Lett. 43 (4) (1998) 476–481.
[10] G. Phillies, G. Benedek, N. Mazer, Diffusion in protein solutions at high concentrations: a study by quasielastic light scattering spectroscopy, J. Chem. Phys. 65 (1976) 1883.
[11] S. Longeville, W. Doster, G. Kali, Myoglobin in crowded solutions: structure and diffusion, Chem. Phys. 292 (2-3) (2003) 413–424.
[12] G. Scatchard, A. Batchelder, A. Brown, Preparation and properties of serum and plasma proteins. VI. Osmotic equilibria in solutions of serum albumin and sodium chloride, J. Am. Chem. Soc. 68 (1946) 2320–2329.
[13] R. Dorshow, D. Nicoli, The effect of hydrodynamics on the diffusivity of charged macromolecules: application to BSA, J. Chem. Phys. 75 (1981) 5853.
[14] K. Keller, E. Canales, S. Yum, Tracer and mutual diffusion coefficients of proteins, J. Phys. Chem 75 (3) (1971) 379–387.
[15] N. Meechai, A. Jamieson, J. Blackwell, Translational diffusion coefficients of bovine serum albumin in aqueous solution at high ionic strength, J. Colloid Interface Sci. 218 (1) (1999) 167–175.
[16] F. Zhang, M. Skoda, R. Jacobs, R. Martin, C. Martin, F. Schreiber, Protein interactions studied by SAXS: effect of ionic strength and protein concentration for BSA in aqueous solutions, J. Phys. Chem. B 111 (1) (2007) 251–259.
[17] F. Zhang, M. Skoda, R. Jacobs, S. Zorn, R. Martin, C. Martin, G. Clark, S. Weggler, A. Hildebrandt, O. Kohlbacher, et al., Reentrant condensation of proteins in solution induced by multivalent counterions, Phys. Rev. Lett. 101 (2008) 148101.
[18] M. Bée, Quasielastic neutron scattering. Principles and applications in solid state chemistry, biology and materials science, Adam Hilger, London, 1988.
[19] G. Squires, Introduction to the Theory of Thermal Neutron Scattering, Cambridge University Press, Cambridge, U.K., 1978.
[20] J. Dhont, An Introduction to Dynamics of Colloids, Elsevier Science, 1996.
[21] A. Fick, Ueber Diffusion, Annalen der Physik und Chemie 170 (1) (1855) 59–86.
[22] W. Doster, S. Longeville, Microscopic diffusion and hydrodynamic interactions of hemoglobin in red blood cells, Biophys. J. 93 (4) (2007) 1360–1368.
[23] G. Vineyard, Scattering of slow neutrons by a liquid, Phys. Rev. 110 (5) (1958) 999–1010.
[24] D. Carter, J. Ho, Structure of serum albumin, Adv. Protein Chem. 45 (1994) 153.
[25] B. Frick, M. Gonzalez, Five years operation of the second generation backscattering spectrometer IN16: a retrospective, recent developments and plans, Physica B: Physics of Condensed Matter 301 (1-2) (2001) 8–19.
[26] ILL (Ed.), http://www.ill.eu/instruments-support/instruments-groups/yellow-book/. The ILL YellowBook, ILL, Grenoble, 2008.
[27] F. Mezei (Ed.), Neutron Spin Echo, Lecture Notes in Physics, 128, Springer, Berlin, 1980.
[28] J. Perez, J. Zanotti, D. Durand, Evolution of the internal dynamics of two globular proteins from dry powder to solution, Biophys. J. 77 (1) (1999) 454–469.
[29] S. Busch, W. Doster, S. Longeville, V. Sakai, T. Unruh, Microscopic protein diffusion at high concentration, in: MRS Bulletin. Quasielastic Neutron Scattering Conference, 2006, pp. 116–117.

[30] B. Armstrong, Spectrum line profiles: the Voigt function, J. Quant. Spectrosc. Radiat. Transfer 7 (1) (1967) 61–88.
[31] F. Schreier, D. Kohlert, Optimized implementations of rational approximations—a case study on the Voigt and complex error function, Comput. Phys. Commun. 179 (7) (2008) 457–465.
[32] J. Végh, Alternative form for the pseudo-Voigt peak shape, Rev. Sci. Instrum. 76 (2005) 056107.
[33] A. Gaspar, M. Appavou, S. Busch, T. Unruh, W. Doster, Dynamics of well-folded and natively disordered proteins in solution: a time-of-flight neutron scattering study, Eur. Biophys. J. 37 (5) (2008) 573–582.
[34] W. Häussler, Neutron spin echo studies on ferritin: free-particle diffusion and interacting solutions, Eur. Biophys. J. 37 (5) (2008) 563–571.
[35] E. Verwey, J. Overbeek, Theory of the Stability of Lyophobic Colloids, Elsevier, Amsterdam, 1948.